JKAU: Eng. Sci., Vol. **33** No. 1, pp: 65 – 82 (1444 A.H. / 2023 A.D.)
Doi: 10.4197/Eng. 33-1.5

Performance of a refurbished unmanned combat air vehicle model with trailing edge blowing

Khalid A Juhany and Mahmood Khalid*
Aerospace Engineering, King Abdul Aziz University, Jeddah, Saudi Arabia

Abstract. A CAD Unmanned Combat Air Vehicle (UCAV 1303) model is constructed from the surface geometry information gleaned from different publications. A simple C- grid is constructed for the purpose of studying the effect of a sheet of ejection jet installed at the thicker portion of the trailing edge to investigate possible effects it could have upon the aerodynamic lift and drag of the UCAV 1303 model. The blowing seemed to improve the lift and make a marginal improvement upon drag.

***Keywords*:** Blowing, CFD, UCAV, Aerodynamic Performance, Turbulence Models, Blended Wing Body Configurations.

1 Introduction

Blended wing body aircraft configurations have been gaining interest both for commercial and military industrial applications. For civilian markets the blended wind body shapes offer larger and spacious passenger cabins with smoother and more comfortable flight prospects, whereas for military applications such stealthy configurations as the Unmanned Combat Air Vehicle UCAV 1303 with comparatively small radar signatures present obvious advantages in hostile encounters. Such blended wing body UCAV's become even more attractive when a pilotless vehicle is damaged without recovery owing to a military mishap. Under both type of applications, the primary focus remains a more streamlined aerodynamic design with elimination of traditional flight control surfaces at the empennage leading to considerable weight savings and reduction of aerodynamic interference. The classic tube and wing design is effectively replaced with a delta wing which

* Corresponding author: mkholid@kau.edu,sa

smoothly blends with the central cylindrical shape to result in the blended wing-body configuration. This document contains results from a numerical study on a blended wing body UCAV 1303 computational model constructed from geometric information obtained from different publications. This UCAV 1303 model was then rigged inside a *Pointwise* grid generator to produce a simple 4 block C – grid which other than enveloping the above model also included the string mount and other flow field details stretching from the wing tips to far field and other regions in the downstream directions. A further mini-block was subsequently inserted in between the two main grid folds to accommodate the blowing slit added at a section of the trailing edge. The accuracy of the numerical model was first authenticated by conducting Navier Stokes based flow simulations at Reynolds number of $Re = 10.4 \times 10^6$ at Mach numbers of M = 0.25 to 0.85 with angles of attack ranging from $\alpha = 2.1^O$ to 10^O. The computational simulations were conducted using an in house algorithm. It was learnt, that not only the model had been produced with satisfactory accuracy, but also that the present computations were as good as the results quoted in various publications. With confidence of these results, a flow ejection scheme was applied at the trailing edge of a portion of the wing. It was learnt that the blowing leads to increasing lift and a noticeable drop in the aerodynamic drag.

1.1 Background

The idea of blended wing body (BWB) aircraft configuration whether for civil or military applications as in UCAV's has been around for a better part of at least 2 decades. Leibeck [1] investigated the blended wing body for transport aircraft back in 2003 and showed a 15% reduction in weight together with 27% reduction in fuel burn per seat for an 800 passenger airliner with a range of 7000 n.m. Other reports by Warwic [2] and Reim [3] point to continuous attention of aerospace giants, Airbus and Boeing in this discipline. Without an emphatic vertical tail, the BWB design suffers from lateral stability challenges and Royson and Khalid1 [4] investigated this issue using numerical techniques.

The UCAV 1303 aircraft design has been studied at length both in wind tunnel campaigns as well as in CFD based simulations conducted at various research labs. Perhaps the first serious wind tunnel study was reported by Bruce [5] who carried out high Mach number measurements on this model. Other low speed wind tunnel studies on UCAV 1303 have been reported by McPharlin et al [6] who investigated the leading edge flow separation on the UCAV 1303 and the effects of leading edge radii. Of course all of these measurements remain proprietary and are not available to researchers at large. One of the first CFD based simulations were carried out at the Institute for Aerospace Research of Canada by Zhang et al [7] who made extensive use of Spalart-Baldwin-Barth, Spalart-Allmaras and Menter SST turbulence models for viscous coupling in Navier-Stokes based simulations with NPARC and FLOWER CFD codes. Comparison of the computed results showed reasonably acceptable agreement with measurements for the inwards chord wise pressure distributions. For the pressure distribution near the wind tip, the comparisons were rather inconclusive as the measured data shown was very brief. The computed viewgraphs also showed a decidedly separated flow from near the leading edge forming a leading edge vortex (LEV) particularly at higher angles of attack $\alpha \geq 4^O$. Other UCAV 1303 model performance validations were carried in Canada by Wong [8] and in UK and Australia by Arthur and Petterson [9] and Brett et al [10] respectively. Most important feature

of these studies was the successful comparison of aerodynamic force components and pitching moments from wind tunnel and numerical simulations. Comprehensive flow visualization studies highlighted the flow separation and transition evoking regions on the top surface of the UCAV 1303. These results confirmed the viability of the UCAV 1303 as a successful flight vehicle. Another paper by Ganglin [11] which discussed the flight attributes of the UCAV 1303 in terms of aircraft payload, range, endurance, propulsion requirements and other mission criteria at some length also carried out successful comparisons between CFD based simulations and wind tunnel measurements at China Aerodynamics Research and Development Center, (CARDC).

Other work on UCAV includes even lower speed comparisons in the range of u ≤ 15 in/s and other experimental work studying fundamental flow aerodynamics on the model surface. Such low speed water tunnel experiments have been reported by Sosebee [12] and Medford [13]. where colored dye was used to inspect the flow patterns and other balance measurement were taken to study the loads. Other wind tunnel Pressure Sensitive Paint (PSP) based pressure plots and force measurements at a higher speed of u = 50 m/s were reported by Shim and Park [14].

Since the blended wing body configurations lack the presence of the classic control surfaces available in the traditional empennages, it is imperative to come up with auxiliary control mechanisms to exert proper control authority. The present computational simulations are particularly focused on using blowing at the portions of the trailing edge to impart appropriate moments to control the aircraft. Other work reported in literature to understand the behavior of UCAV 1303 configuration subject to external inputs includes the experimental work by Lopera et al [15], which examined the control response on a UCAV 1303 subject to plasma actuators. Lee et al [16] examined response to seven arrays of synthetic jets mounted at span wise locations at the leading edge. They carried out comprehensive comparisons of force, moment, and surface pressure measurements against computations. They found that that the pitching moment was clearly affected by actuating locations and some cases were more effective than the full actuation case even with one actuator. Again Williams and Siedel [17] used a pair of actuators at the leading edge and mid-span of a generic tail less delta winged UCAV and found that the application of mass flow did indeed lead to increased CL, CM and the all-important L/D values. The flow conditions for their studies were M = 0.2, $-4^O \leq \alpha \leq 26^O$ with the sideslip angle in the range $-10^O \leq \beta \leq 10^O$ at a Reynolds number of 730,000. The blowing coefficient $\frac{\int \rho u^2 dA}{\rho_\infty U_\infty^2}$ was varied from $C_\mu = 0.0006$ to 0.0149.

1.2 Preparation and construction of the UCAV Model

The detailed numerical surface information to construct the UCAV 1303 model for a computational study is not so easily available. The geometric information such as the wing span, chord length as well as the leading and trailing sweeps are readily tabulated in various UCAV 1303 publications. The primary base geometry information itemized in Table 1 was taken from Ref 9.

Table 1 UCAV 1303 Basic Geometry

Parameter		Model M2445
Span	m	1.5240
Reference length (mac)	m	0.5397
Reference (wing) area	m	2 0.6021
Leading edge sweep	O	47

Trailing edge sweep	O	30
Aspect ratio		3.857
Moment reference	m	0.45885
(at 35% in wing plane)		Aft of apex
Moment Z location	m	0.35 down

It had been further stipulated in the paper by McPharlin et al [6] that the baseline 1303 configuration was not cambered and had NACA 64A thickness profiles varying from 12% thickness/chord (t/c) at the centreline, to 10% t/c outboard of the main landing gear bays, down to 8% t/c from the inboard crank to the wing tip. Based on the coordinates of the NACA 64 airfoil as shown in Figure 1, and the aforesaid local thickness to chord information, the span wise wing shape was easily arrived at by referring the actual leading and trailing edges to remain within the limits as defined by a blown up version of Figure 2 from Petterson [18]

.

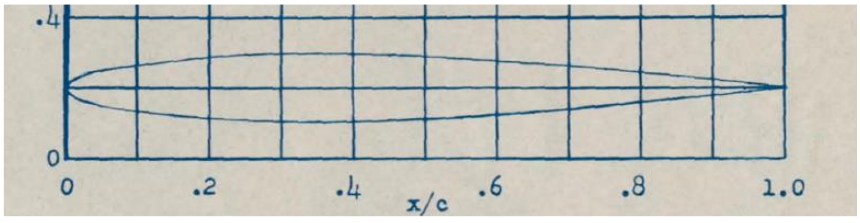

Figure 1 NACA 64A Aerofoil stacked in span wise direction

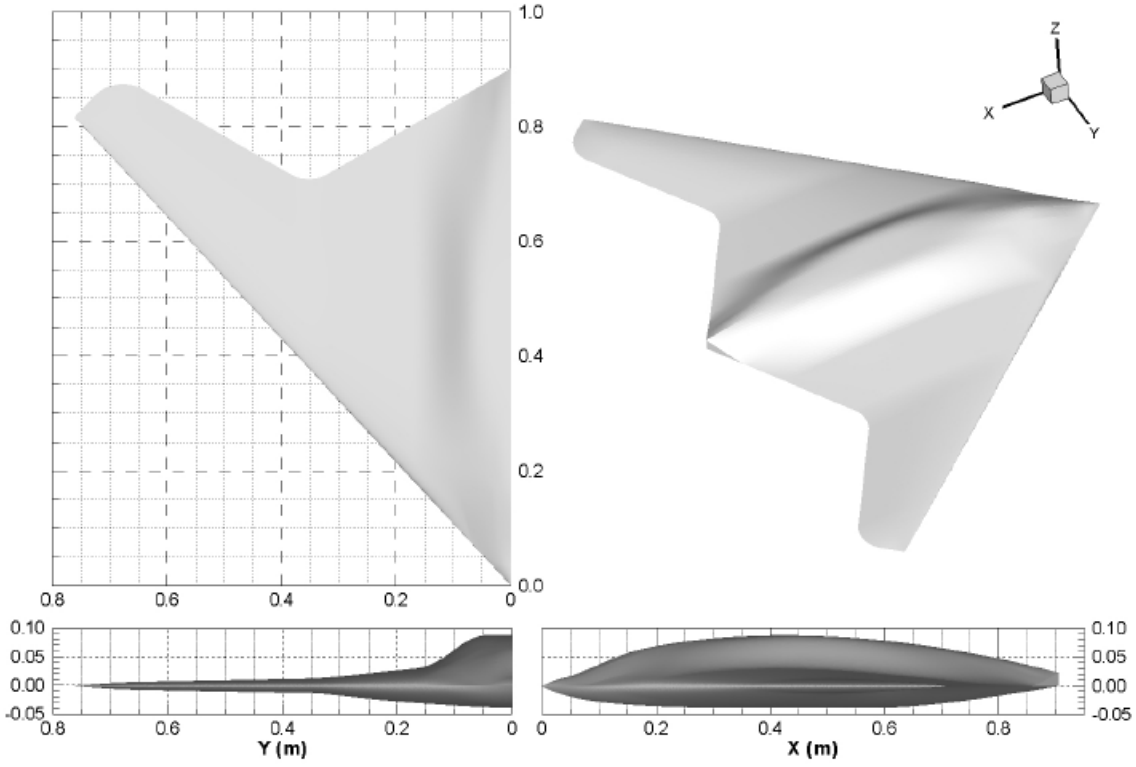

Figure 2 Illustration Showing the Span wise Thickness to Chord

The centerline ogive shape was then blended in with the successively distributed airfoil along span wise direction using CATIA and CAD based facilities. Some numerical fixing was required to obtain the leading edge geometry as recommended in Wong et al [8]. The radii were thus painstakingly adjusted upon each airfoil leading edge by replacing the original portion of the curvature with the new profile of the selected span wise locations. Sometimes the extrapolating surfaces across airfoil cross sections did not abut very smoothly and had to be iteratively surface splined in order to produce a continuous geometry. Occasionally the abutting did not work too well and left the telltale signs of a 'crinkle' at the joint

.

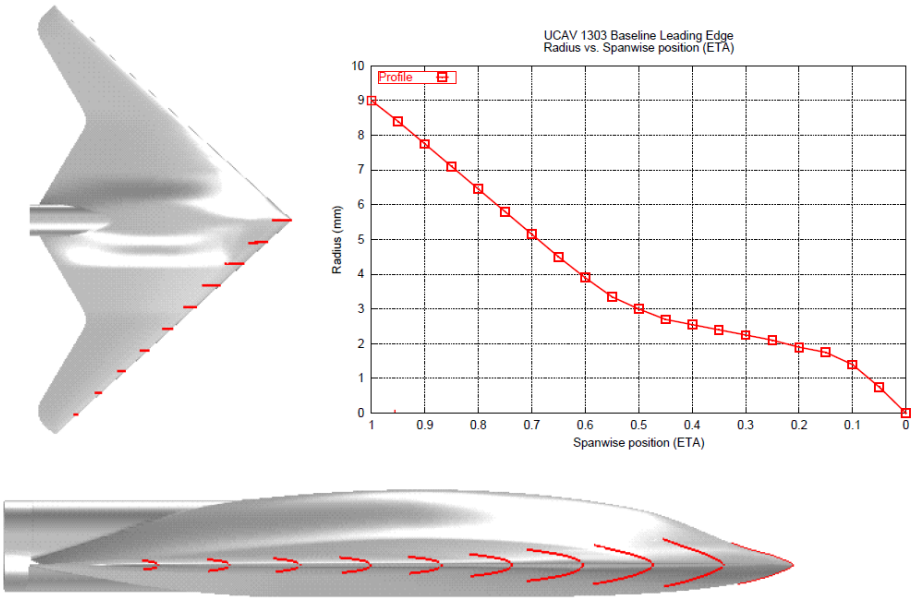

Figure 3 Span wise leading edge radii distribution for UCAV 1303

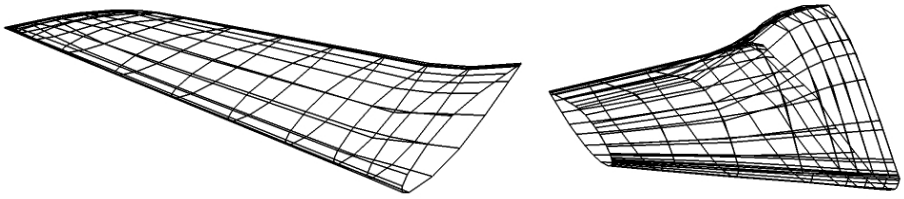

Figure 4 Wireframe geometry of the inward and outward portions of the UCAV 1303

The wireframe of the surfaces for the complete wing for both inner portion and outer region where the successive airfoils were blended with the centerline geometry are shown in Figure 4. Once all the interlocking and abutting surfaces were cleaned and accurately defined a smooth wing shape shown in Figure 5 was readily available. A 3D C-grid type of mesh was created around the complete configuration. Where the mesh could not adequately cover of the surfaces in between the cylindrical surfaces near the sting mount and also behind the sharp trailing edge, simple rectangular prismatic grid blocks were inserted in between the main folding C-grid (shown in Figure 6) which traversed the chord wise geometry from the far downstream on the under surface and doubled back at the leading edge and traveling back to the far down stream.

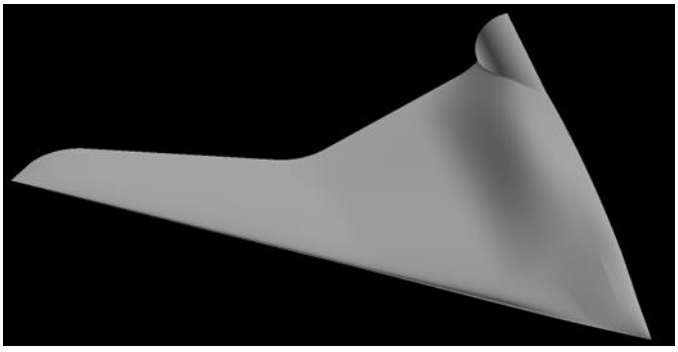

Figure 5 Complete CAD Model UCAV 1303

The additional blocks were required where the immediate regions behind the wind trailing edge and beyond the wing tip had to be resolved more accurately using finer grids. The blowing boundary condition was instrumented using a locally thicker trailing edge. A localized mesh of dimensions 17 X 49 X 84 was inserted in between the folding mesh at the trailing edge. The far downstream location was kept at a distance of about 10 fuselage lengths aft of the fuselage trailing edge. The far field in front and in normal direction was kept a distance of about 6 fuselage lengths from the model. The grid traverses in the span wise direction from the centerline, around the blended region and then on to the wing tip and so on to the far field with mesh lines becoming increasingly coarser from the reflection plane boundary.

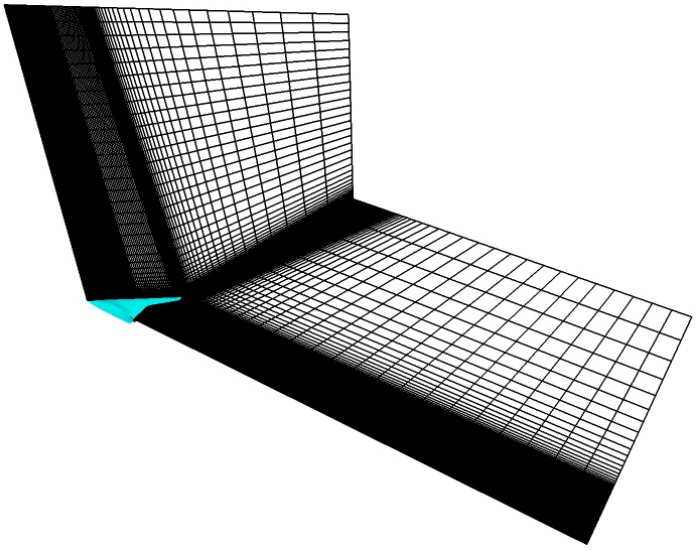

Figure 6. The main mesh 201X131X67 for the UCAV Model 1303

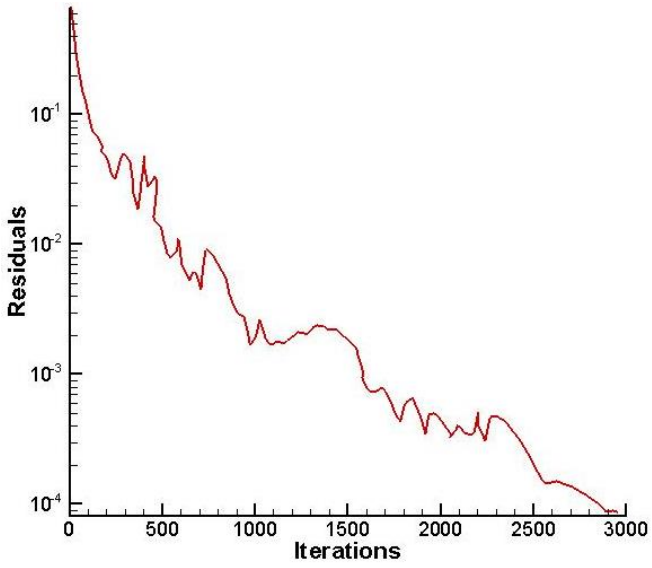

Figure 7 Convergence history of a typical execution at M = 0.86, Re = 10.4 X^6 and $\alpha = 2.1^O$

1.3 Computational Method

An in-house Navier Stokes code was used for the present CFD simulations. The Navier-Strokes equations in the algorithm are formulated along implicit approximate factorization scheme using Beam and Warming [18] scheme with non-linear terms being treated with local time linearization. Other spatial terms in the code are cast as a 3 point backward implicit time differenced and second order finite differenced spatial expression. In order to achieve non-linear stability, explicit and implicit dissipation is added to the algorithm. The code is equipped to treat a variety of boundary conditions including Euler/Slip, No-slip/viscous, free stream upstream and far field downstream conditions. The code uses an extrapolation estimation to reach the far field condition. The code uses interpolation of flow conditions at the boundaries to calculate the overlapping or abutting boundary condition. For a particular blowing condition, it invokes an Euler like treatment fixing the flow conditions at the boundary to the prescribed value while forcing the adjoining cells on all sides to adjust conditions to match the situation at the boundary. In order to facilitate quicker convergence second and fourth order dissipation coefficients of 0.25 and 0.64 were used in the appropriate terms of the digitized equations. A typical convergence trace for a Mach Number of M = 0.85 at a Reynolds number of 10.4 $X10^6$ and $\alpha = 2.1^o$ is shown in Figure 7. It is observed that convergence rate is quite rapid up to about 3000 iteration, beyond which point it tends to slow down without noticeable change in residual computed flow values. The residual drops by four orders of magnitude in first 3000 iterations. While a preliminary study using the Baldwin-Barth and Spalart – Allmaras model had yielded results typical of what had been observed by other authors, the computations using the two equation k- ω(Wilcox) [19] model, particularly at higher Mach number provided a much better agreement.

1.4 Discussion of Results

1.4.1 Solid Body Calculations

CFD based computations were carried at Mach numbers of M = 0.25, 0.35 and 0.85, at angles of attack in the range $\alpha = 0.31^O$ to 10^O at Reynolds

number of Re = 10.4X10^6. The complete investigation included solid body computations to make sure that our simulation results matched satisfactorily against the existing solid body simulations as well as powered runs with outflow at the trailing edge ranging from a low value of the C_μ ($\frac{\int \rho u^2 du}{\rho_\infty U_\infty^2}$) $= 0.0006\ to\ 0.015$. The low ejection flux value was only used as a pilot run to make sure that the algorithm adequately handled the blowing boundary condition at the trailing edge. It was well understood that such a large and bulky vehicle could only respond to sizeable blowing rates. Figure 8 shows the first validation results of pressure coefficient at M =0.25, $\alpha = 3^0$ and Re = 10.4 X10^6, amongst different simulations from NASA, DSTO and present KAU calculations. The results from NASA as reported by Wong [8] and present KAU results on the left using same legend scale match each other quite well. The results from DSTO [8] on the extreme right allowing for an enlarged scale too by and large match the two results on the left.

The next flow field investigation dealt with a slightly higher angle of attack $\alpha = 4.6^0$ with Mach number still at M = 0.25 and Re = 10.4 X10^6. The equivalent graphic flowfield pressure distributions taken from NASA, DSTO in Ref [8] and KAU are shown in Figure 9. It appears that the results when appropriately resolved for different scales show reasonable similarity with each other.

A more comprehensive comparison of present computations against COBALT and Jupiter [9] algorithms is also carried out. As outlined in Ref [9], COBALT is a USAF unstructured grid based CFD code, which uses a cell-centred finite volume approach applicable to arbitrary cell types. The spatial operator uses an exact Riemann solver, least squares gradient calculations using QR factorization to provide second order accuracy in space and TVD flux limiters to limit extremes at cell faces. In the context of the present results, the COBALT was run using the Spalart-Allmaras model with corrections for rotational flow (SARC) and Menter's blended k-w shear-stress transport (k-w-SST) two-equation model. Jupiter is an explicit, cell-centred method designed to operate on meshes containing arbitrary polyhedral and was developed in UK jointly by BAE Systems, ARA, Airbus and QinetiQ. Jupiter was executed using k-ω or the k-g model. K-g model is essentially the same as the k- ω model, where the value of ω is replaced with the expression $\omega = \frac{1}{C_\mu g}$ and g takes up values in between 0.5 to 0.8. Where appropriate NASA's results from the OVERFLOW code and DSTO's Fluent based results are also quoted for comparisons. OVERFLOW was run using Menter – SST and Fluent with k-ω SST two equation turbulence models. The actual turbulence models used in an execution is duly noted in the comparison if its results show notable deviation from other closer results.

Axial pressure distribution comparisons at M =0.25, $\alpha = 4.6^0$ and Re = 10.4 X10^6 are shown at three chord wise stations $\eta\left(\frac{y}{b/2}\right) =$ 0.4, 0.6 and 0.8. The experimental values were directly mapped from Reference 9. Unless mentioned specifically the collective data for 5 different models as indicated in each graph refers to (SST, SARC, k-g original, k-g with transition and k-g transition models. It should also be noted here that results from the above mentioned DSTO and NASA computations which use SST k-ω and Menter SST turbulence models in Reference [8], although not indicated separately, coincided almost exactly with the results from these 5 turbulence models.

In most cases the predictions remain very close to the experiment with the present results giving very good comparison with other computations and experiment. At station η = 0.6 the present results trace the experiment most closely. The use of original k-g turbulence model for the span wise case c (η=0.8) records an inexplicable peak on the top surface at x/c(local) = 0.55, which is at total variance with experimental trend. Other results from NASA and DSTO, although not mentioned in the legend, remain well within the line thickness of the present results. Also note in Figure 10 that the flow on the UCAV 1303 surface as recovered from the present computations remains completely attached to

the model, as has also been noted in References [8,9,10,20].

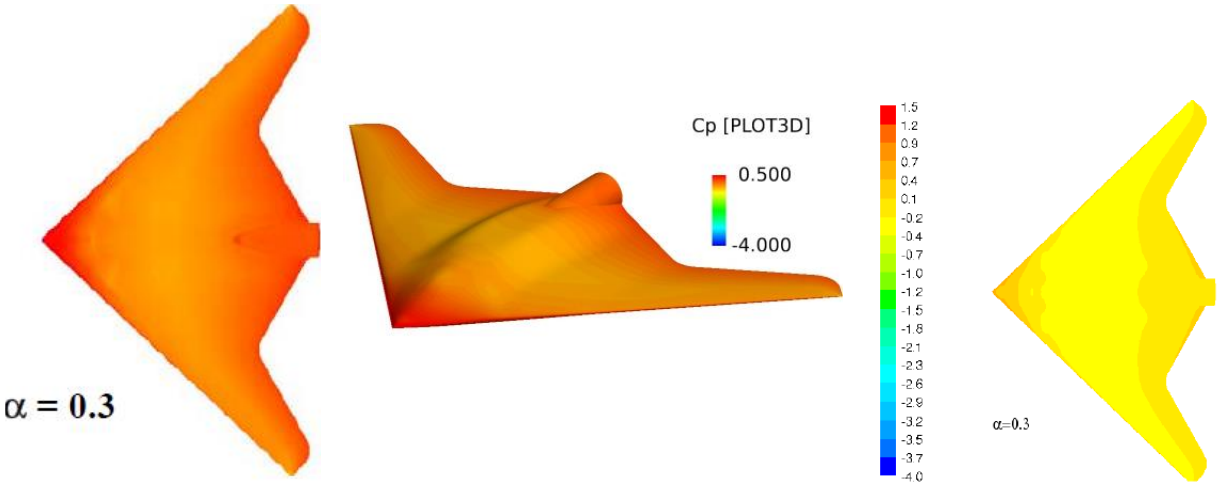

NASA KAU DSTO

Figure 8 shows the pressure coefficient at M =0.25, $\alpha = 3^0$ and Re = 10.4 X10^6

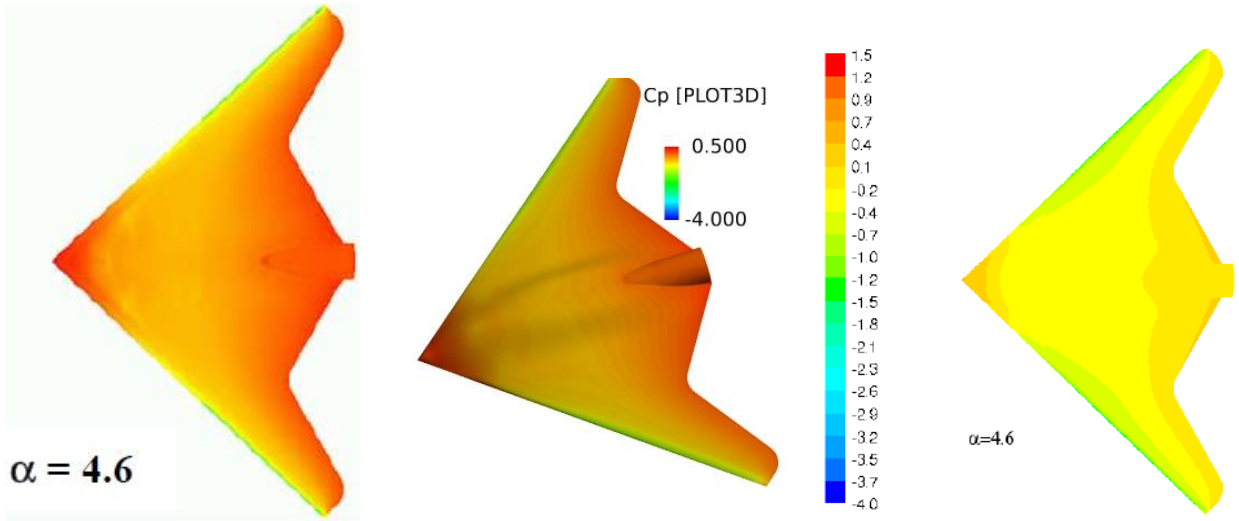

NASA KAU DSTO

Figure 9 shows the pressure coefficient at M =0.25, $\alpha = 4.6^0$ and Re = 10.4 X10^6

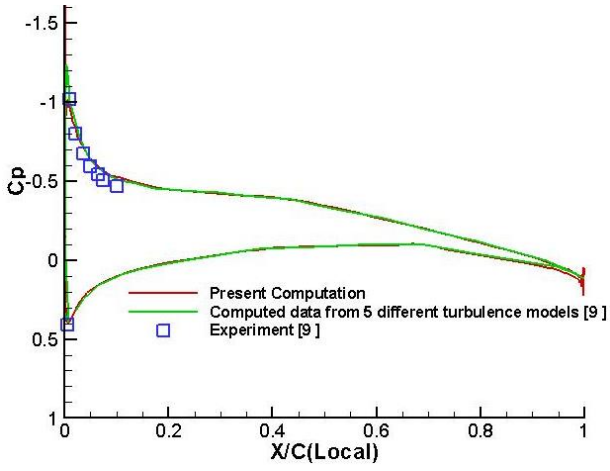

(a)

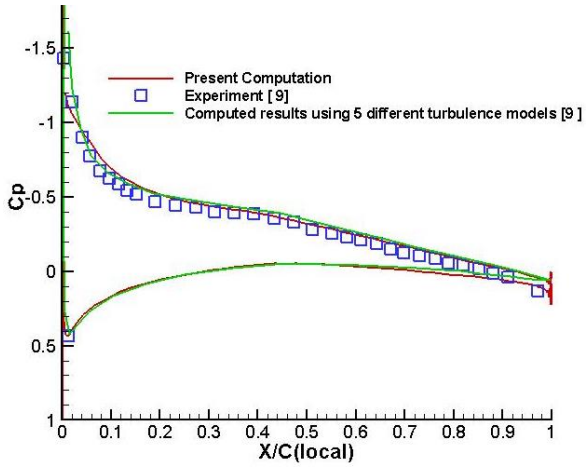

(b)

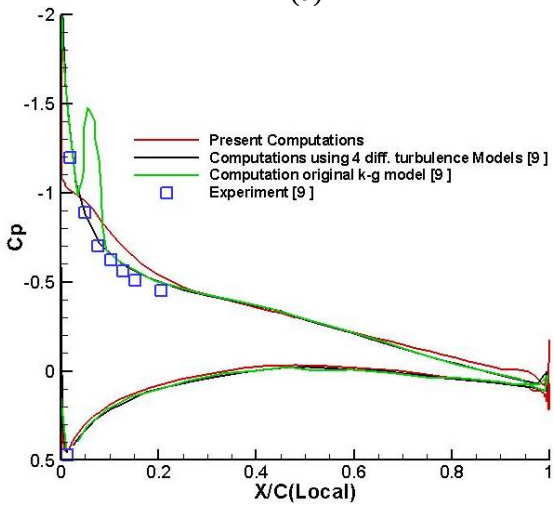

(c)

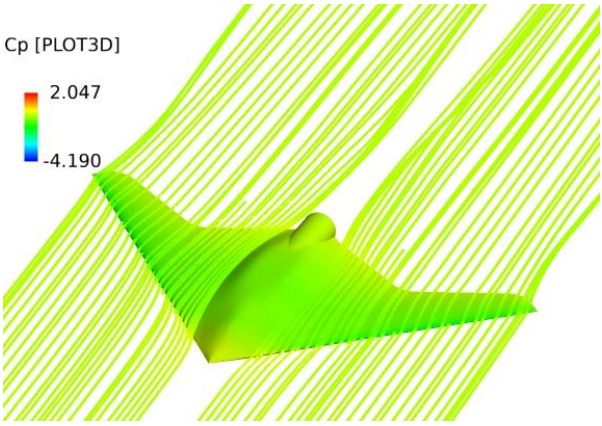

(d)

Figure 10 Cp at M =0.25, $\alpha = 4.6^0$ and Re = 10.4X10^6 at span wise station (a) η = 0.4, (b) η = 0.6, (c) η = 0.8 and (d) shows surface streamlines

Further span wise comparison of the flow field pressure distribution as shown in Figure 11 was carried out at a higher Mach number of M = 0.35, $\alpha = 10.^0$ and Re = 8.0 X10^6. Close to the centerline almost all the codes gave pretty good agreement with the experiment, especially FLOWER based computations using Menter SST turbulence model near the front. However, present k-ω based computations especially on the upper surface provide the best outcome of all the available cases. IAR computation for the span wise station η= 0.3 shows a little peak in the pressure trace at x/c(Local) = 0.5 The lower surface results, however, are well matched amongst all the cases.

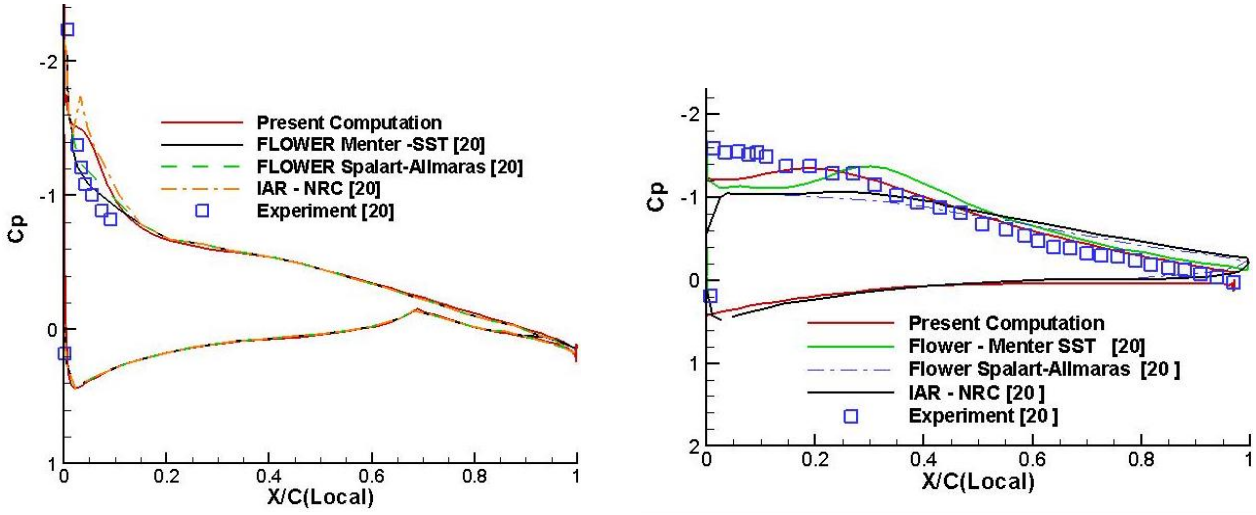

(a) (b)

Figure 11 Cp at M =0.35, $\alpha = 10^0$ and Re = 8 X10^6 at span wise station (a) η = 0.3 and (b) η = 0.6

The streamlines at such high angles of attack understandably show massive flow separation immediately starting from the leading edge of the model. Despite regions of separated flow at such high angle of attack, the turbulence models have indeed done well in resolving the flow. Figure 12 shows the separated streamlines from at least two such computations. It was learnt during the course of such studies that flow starts separating at the tip end starting at angles of attack $\alpha \geq 5^O$. In both viewgraphs of Figure 12 the model itself shows the surface pressure distributions, whereas the streamlines in the left figure are displayed in grey while those in the right figure are colored by Mach number.

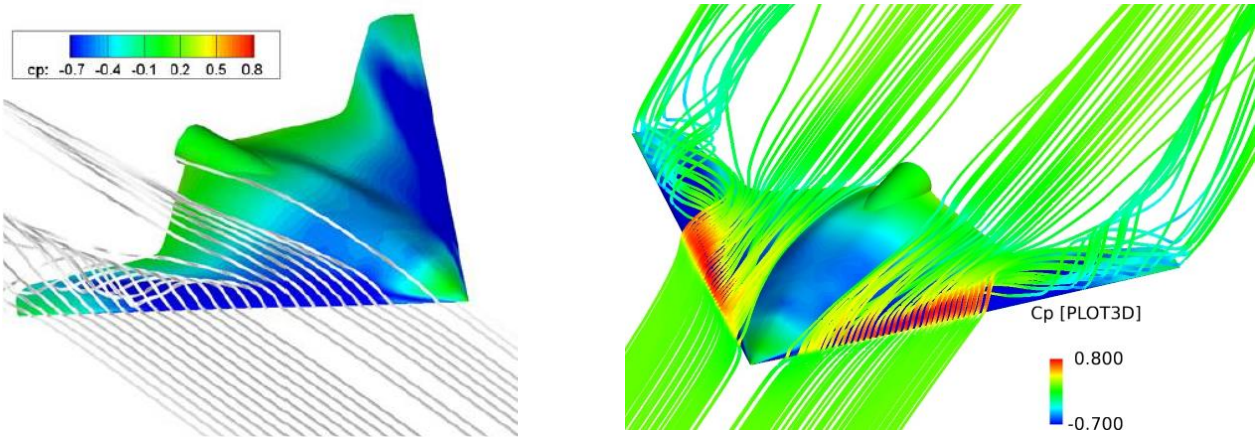

(a) (b)

Figure 12 Surface stream lines from (a) Reference[20] and (b) present computations at M = 0.35, $\alpha = 10^0$ and Re = 8 X10^6

To validate the code at an even high transonic Mach number, one further computation was performed where the data was available in literature[7,20] for M = 0.85, α = 2.1^{O} and Re = 12X10^{6}. The comparison is shown in Figure 13.

It appears that except for IAR[20], which shows a strange spike at x/c = 0.05 for $\eta = 0.3$ station most results are bunched comfortably close to each other. For the η = 0.6 case on the right-hand side, both FLOWER based computations using Menter-SST and Spalart-Allmaras turbulence models under predict the shock at x/c(Local) = 0.5. The IAR results come close, but the present computations have resolved the shock almost perfectly. The increase of Mach number, however, does not transform the separation regime too drastically provided that the Mach number is low. It is observed from both results in Figure 14 that the streamlines remain well behaved and fully attached at the present flow conditions, M =0.85, $\alpha = 2.1^{0}$ and Re = 12X10^{6}.

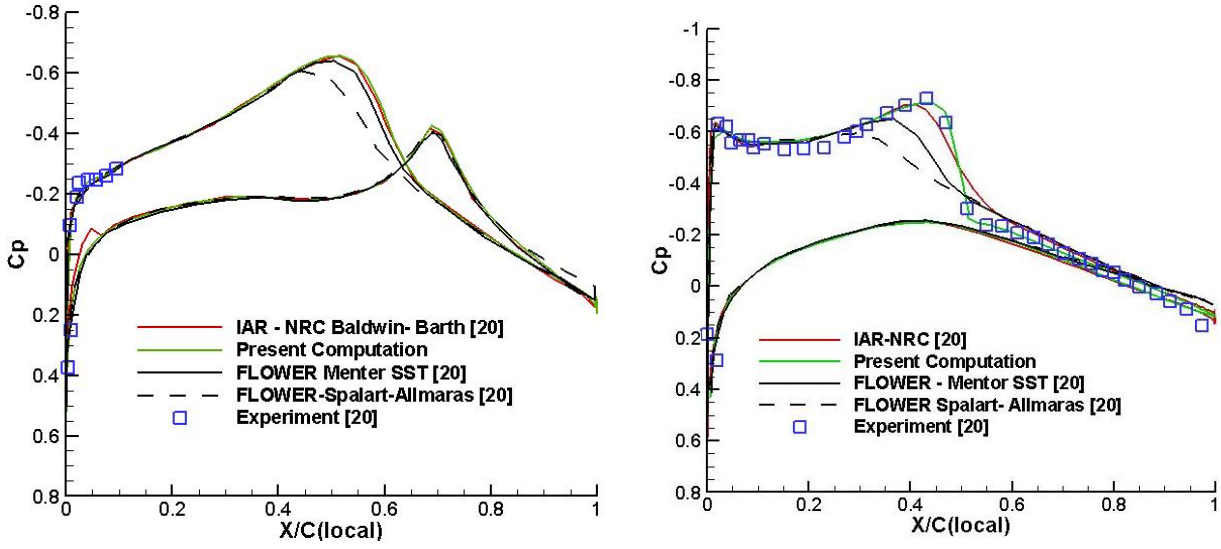

(a) (b)

Figure 13. Cp at M =0.85, $\alpha = 2.1^{0}$ and Re = 12X10^{6} at span wise station (a) η = 0.3 and (b) η = 0.6, present k-ω based.

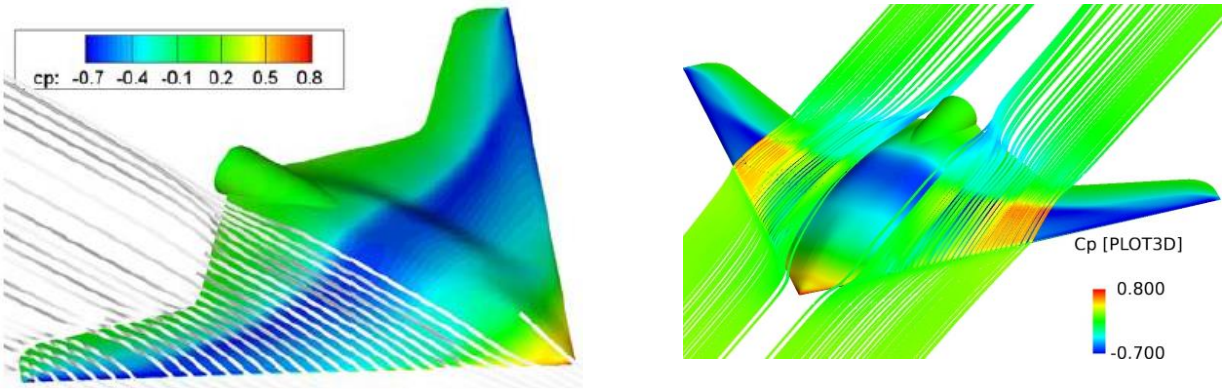

Figure 14 Surface stream lines from (a) Reference[20] and (b) present computations M = 0.85, $\alpha = 2.1^0$ and Re = 12X10[6]

1.4.2 Power-On Flow Ejection at the trailing Edge

The trailing edge of the UCAV model was reconstructed with an additional thickness to facilitate the trailing edge blowing. A suitable slit grid was inserted into the trailing edge. For the present computations only one thickness was tested, however, there is a provision in the topology to adjust the thickness depending upon the required flux momentum. The portion of the model where this blowing condition is applied is shown in Figure 15. The flow efflux geometry can be readjusted by changing the dimensions of this insert which slides into the trailing edge of the wing. Depending upon the required thickness of the upstream end of this mesh, the insert would abut more deeply into the existing wing. Contiguous block condition would prevail if no blowing condition existed at the boundary. The span wise blowing can be controlled by adjusting the span wise 'J' index of the IJK notation of the local block insert. All of the above computations were repeated under power-on conditions with varying momentum flux at the trailing edge. To validate the blowing condition in the first instance a momentum efflux rate of $C_\eta = \frac{\int \rho u^2 du}{\rho_\infty U_\infty^2} = 0.0007$ was used to make sure that the code would run successfully. Higher blowing coefficients would be used for the remaining study. The integrated values for C_L and C_D, as obtained for this low value of $C_\eta = 0.0007$ were then superimposed upon the equivalent solid body C_L and C_D polars from the present computations and other results from Ref[9]. This comparison is shown in Figures 16.

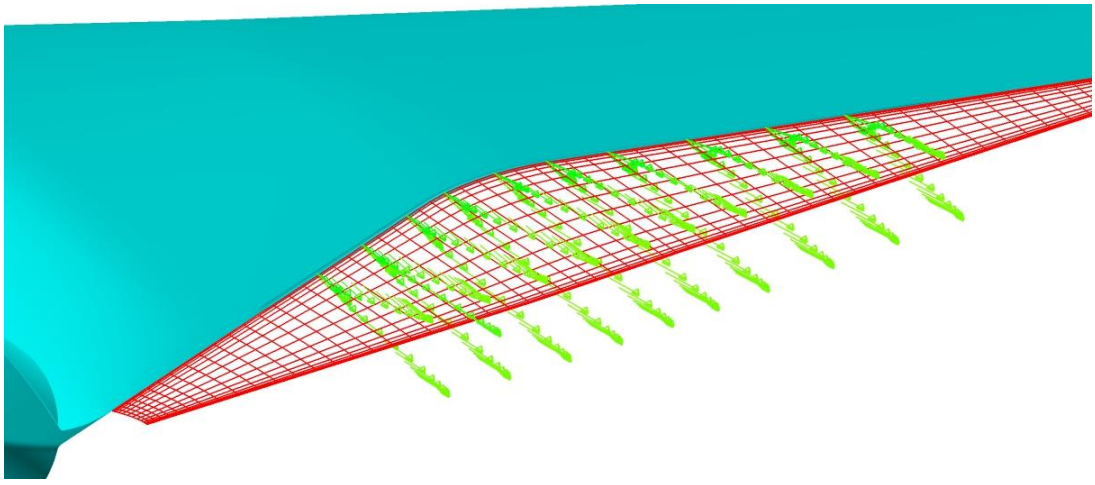

Figure 15 Trailing edge mesh aft of the UCAV 1303 Model

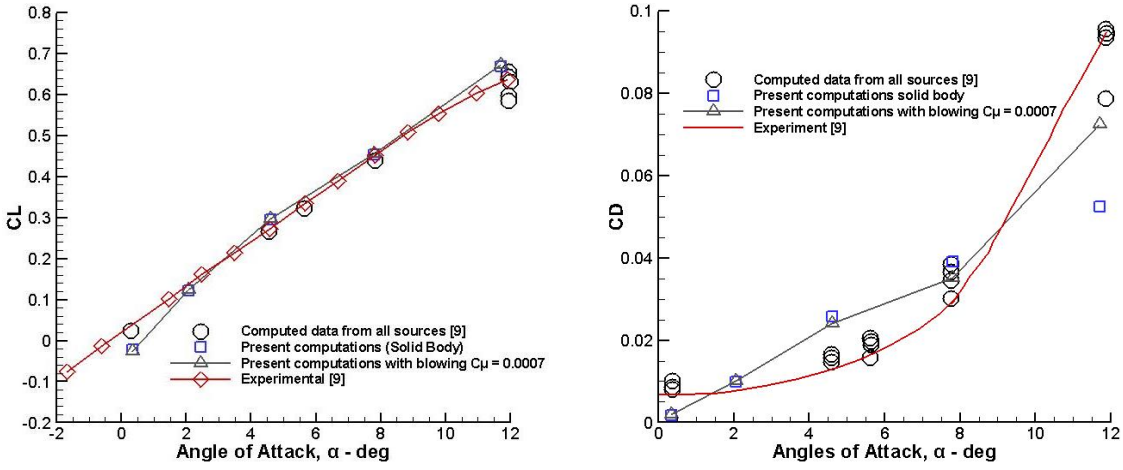

Figure 16 Lift (left) and Drag (right) polars the UCAV 1303 Model

The lift and drag polars in Figure 16 include the computed and measured data from Arthur and Petterson[9] . The computed data was obtained from at least three international partners including UK, US and Australia who had used no less than seven turbulence models to obtain these results. The measurements were mostly recorded in the UK 5 meter Farnborough tunnel. The present CL results sit comfortably with all other measured and computed data in the angle of attack range $0° \leq \alpha \leq 12°$. At the lowest angle of attack $\alpha = 0.33°$ the CL values are somewhat under predicted. The small value of blowing at the trailing edge, $C_\eta = 0.0007$, used here only to exercise the blowing boundary condition has made very little difference to the lift profile.

The coefficient drag which is presented on the right hand side of Figure 16 is extremely difficult to compute especially when the flow is separated on the model surface as indeed was the case for the present model where there was notable evidence of flow separation for angles $\alpha \geq 5.5°$. Both, pressure distributions and surface flow velocities are affected when the flow is separated and both pressure integration $\int C_p dx$ and shear stress $\int \mu \frac{du}{dy}_w dx$ used in the calculation of CL and CD become compromised in an increasingly complex flow field. Thus the drag is over predicted in the regime, $2° \leq \alpha \leq 8°$. Again the very nominal value of the trailing edge blowing has only made a very marginal difference to the coefficient of lift.

Conclusion

The CAD based geometry of the UCAV 1303 constructed from very basic information in literature has performed successfully in present investigation.

The solid body results are in satisfactory agreement with results from computations carried out in the leading world centers.

The very low values of the blowing coefficient used in present study seem to have little difference to the aerodynamic loading. It is anticipated that larger value of the blowing coefficient $C_\eta \geq 0.01$ may lead to a more convincing validation of the procedure.

Disclosures

There are no conflicts of interests involved in conducting the work in this article. The work was completed entirely from KAU resources using in-house CFD algorithms.

Acknowledgments

The authors are grateful to the Deanship of the Faculty of Engineering of the King Abdul Aziz University for their continued financial support and encouragement in the course of this work

Code, Data and Material Availability

All data and results presented in this paper would be readily available to research community. The CFD code developed by the KAU scientists and used in this paper is subject to KAU University IP constraints and would need necessary approval before release.

References

[1] **Liebeck, R.H**. (January–February 2004). "Design of the Blended Wing Body Subsonic Transport". AIAA Journal of Aircraft. **41** (1). pp. 10–25.

[2] **Warwick, Graham**. "Boeing works with airlines on commercial blended wing body freighter." Flight International, May 21, 2007.

[3] **Reim, Garrett**; "Airbus studies blended-wing airliner designs to slash fuel burn". Flight Global, Feb 11, 2020

[4] **Royson, Paul F. and Khalid, M,** " Lateral-Directional Stability Investigation of a Blended-Wing Body", 10th AIAA Aviation Technology, Integration, and Operations (ATIO) Conference, 13 September 2010 - 15

[5] **Bruce R J.** High Speed Wind Tunnel Tests on the 1303 UCAV Concept. Internal Report, QinetiqQ Ltd, QinetiqQ Farnborough, UK, QINETIQ/FST/TR030214/1.0, 2003.

[6] **McPharlin, S. C., Bruce, R. 1., Hepworth, A. G., Rae, A. 1**., 2003. "Low speed windtunnel tests on the 1303 UCAV concept", QinetiQ/fST/tR02550211.0, QinetiQ Ltd., Farnborough, UK, March, 2003

[7] **Zhang, F., Khalid, M., Ball, N**., 2005. "A CFD based study of UCAV 1303 model", AIAA Paper 2006-4615.

[8] **Wong, M. D., McKenzie, G. 1., 01, M. V., Petterson, K., Zhang, S.**, 2006. "Joint TTCP CFD studies into the 1303 DCAV performance: first year results", AIAA Paper 2006-2984**.**

[9] **Arthur, M. T. and Petterson, K.,** "A computational study of the low-speed flow over the 1303 UCAV configuration", 25th AIAA Applied Aerodynamics Conference, 25 - 28 June 2007, Miami, FL

[10] **Brett, J., Tang, L, Hutchins, H., Valiff, A. and Oii, A.,** "Computation Fluid Dynamics Analysis of the UCAV 1303 Vehicle", 17th Australasian Fluid Mechanics Conference, Auckland, New Zealand, 5-9 December 2010.

[11] **Ganglin, W.,** " Key Parameters and Conceptual Configuration of Unmanned Combat Aerial Vehicle Concept", Chinese Journal of Aeronautics 22(2009) 393-400.

[12] **Sosebee, P. D.** " Flow visualization and detailed load measurements for a maneuvering UCAV 1303",Ph. D Thesis, http://hdl.handle.net/10945/5743, March 2011, Monterey, California. Naval Postgraduate School.

[13] **Medford, M**., "The aerodynamics of a maneuvering UCAV 1303 aircraft model and its control through leading edge curvature change", M Sc Thesis, September 2012, Monterey, California. Naval Postgraduate School

[14] **Shims, H. J. and Park, S. O**., "Low-speed wind-tunnel test results of a BWB-UCAV model"; 7th Asian-Pacific Conference on Aerospace Technology and Science, 7th APCATS 2013, Procedia Engineering 67 (2013) 50 – 58.

[15] **Lopera, J., Ng, T. T., Mehul P. Patel, M. P., Vasudevan, S and Corke, T. C.**, "Aerodynamic Control of 1303 UAV Using Windward Surface Plasma Actuators on a Separation Ramp", 45th AIAA Aerospace Sciences Meeting, 8-11, January, RENO, Navada

[16] **Lee, J., Lee, S. and Kim, C**., "Actuations of Synthetic Jets on a UCAV Planform at High Angles of Attack "; AIAA Aviation, 8th AIAA Flow Control Conference, 13-17 June 2016, Washington, D.C.

[17] **William D. R. and Sidel, J.**, " Crossed-Actuation AFC for Lateral-Directional Control of an ICE-101/Saccon UAV"; AIAA Aviation, 8th AIAA Flow Control Conference, 13-17 June 2016, Washington, D.C.

[18] **Beam RM, Warming RF**. An implicit factored scheme for the compressible Navier–Stokes equation, AIAA Journal, Vol.16, 1978, pp.393–402.

[19] **Wilcox, D.C**. 'Re-assessment of the scale-determining equation for advanced turbulence models', AIAA Journal, Vol. 26, No. 11, 1988, pp. 1311-1320.

[20] **Khalid, M., Yuan, W. and Zhang,F.,** 'A CFD study of UCAV 1303 Baseline Model at Cruise Mach Numbers', 26TH International Congress of the Aeronautical Sciences', ICAS 2008**.**

أداء نموذج محدث لمركبة جوية قتالية بدون طيار ذات نفث خلفي

خالد الجهني ومحمود خالد
هندسة الطيران، جامعة الملك عبد العزيز، جدة، المملكة العربية السعودية

الملخص

تم إنشاء نموذج لمركبة جوية قتالية بدون طيار من معلومات هندسة السطح المستقاة من منشورات مختلفة. حيث تم إنشاء شبكة بسيطة على شكل حرف "C" بغرض دراسة تأثير شريحة نفث رقيقة مثبتة في الجزء السميك من الحافة الخلفية للتحقق من التأثيرات المحتملة التي يمكن أن تحدثها على الرفع والكبح لهذا النموذج، حيث أظهرت النتائج أن النفث الخلفي يحسن من الرفع بينما يحدث تحسنا هامشيا في الكبح.

الكلمات المفتاحية: النفث، ديناميكا الموائع الحسابية ، مركبات جوية قتالية بدون طيار ، الأداء الديناميكي الهوائي ، نماذج الاضطراب ، الأجنحة المدمجة.